The Dependence of Portevin–Le Châtelier Effect on the γ' Precipitates in a Wrought Ni-Base Superalloy

XINGUANG WANG, GUOMING HAN, CHUANYONG CUI, SHUAI GUAN, TAO JIN, XIAOFENG SUN, and ZHUANGQI HU

The dependence of Portevin–Le Châtelier (PLC) effect on the γ' precipitates of the Nimonic 263 alloy in different microstructural conditions has been studied by analyzing the parameters of the tensile curves and the deformation mechanisms. It is shown that the γ' precipitates with different sizes, edge-to-edge interprecipitate distance, and areal number density are obtained by altering the aging time. It is demonstrated that when the mean size of the γ' precipitates is less than 28 nm (aging less than 25 hours), the deformation mechanisms are dominated by APB-coupled a/2⟨101⟩ dislocations shearing the small γ' precipitates and the slip bands continuously cutting the γ and γ' phases. When the γ' size is between 28 and 45 nm (aging time between 25 and 50 hours), the deformation mechanism is controlled by the APB-coupled a/2⟨101⟩ dislocations shearing the small γ' precipitates, the a/6⟨112⟩ Shockley partial dislocation continuously shearing the γ and γ' phases combined with matrix dislocations by-passing the γ' precipitates; If the γ' size over 45 nm (aging time more than 50 hours), Orowan by-passing becomes the main deformation mechanism. Moreover, with increasing the aging time, the critical plastic strain for the onset of the PLC effect increases and reaches a maximum after aging for 50 hours, and then gradually decreases. At last, the dependence of critical plastic strain on the deformation mechanisms is well explained by the elementary incremental strain (γ). The precipitation process of the γ' phase can directly influence the PLC effect by changing the interactions among solutes atoms, mobile dislocations, and forest dislocations.

DOI: 10.1007/s11661-016-3718-x

I. INTRODUCTION

THE Portevin–Le Châtelier (PLC) effect is commonly observed in many alloys during plastic deformation within a certain regime of temperature and strain rate, and it exhibits temporally as continuous serrated yielding in stress–strain curves and spatially as repeated propagation of strain localizations.[1–4] This phenomenon is generally considered to be a plastic instability associated with dynamic strain aging (DSA),[5–9] *i.e.*, dynamic pinning and unpinning interactions between mobile dislocations and diffusing solute atoms.

According to the DSA theory, the concentration and diffusion rates of solute atoms combined with density and velocity of mobile dislocations jointly determine the degree of the PLC effect. The bulk diffusion rate of solute atoms is normally much lower than the velocity of mobile dislocations, so the mobile dislocations cannot be pinned effectively if only the bulk diffusion mechanism of solute atoms is considered. Thus, the vacancy aided bulk diffusion mechanism was proposed by Cottrell.[1] However, this theory cannot explain the alloy system with interstitial atoms, because the diffusion process of interstitial atoms is not necessary by means of vacancy. In view of the discontinuity of the dislocation movement, McCormick *et al.*[2] and Beukel *et al.*[3] proposed a model (MC model) to explain the DSA theory, *i.e.*, the surrounding solute atoms may segregate to the mobile dislocations by bulk diffusion which have been partially prevented by the obstacles, such as forest dislocations and precipitates. The MC model introduces a parameter t_w which is defined as the waiting time of the mobile dislocations at the obstacles, and therefore correlates the mobile dislocations, solute atoms, and forest dislocations together.

Hereto, the micromechanisms of DSA are further clearly expressed. Mulford and Kocks[5] proposed another model, termed as M–K model, to further describe DSA, which has been acknowledged by the following researchers.[6,7] The M–K theory held that solute atoms segregate to the forest dislocations, and then drain by pipe diffusion from the forest dislocations to the mobile dislocations which are obstructed by the forest dislocations and temporarily stop moving. Obviously, both models are consistent in the interaction between the forest dislocations and the mobile dislocations, and the very limited difference between MC model and M–K model is about the solute atoms diffusion modes. In other words, both models considered that the interactions among solute atoms, forest dislocations, and mobile dislocations are the requirements of DSA. In

XINGUANG WANG, GUOMING HAN, and SHUAI GUAN, Research Assistants, and CHUANYONG CUI, TAO JIN, XIAOFENG SUN, and ZHUANGQI HU, Professors, are with the Institute of Metal Research, Chinese Academy of Sciences, Shenyang 110016, P.R. China. Contact e-mail: chycui@imr.ac.cn
Manuscript submitted November 1, 2015.
Article published online August 15, 2016

the previous work, other influencing factors for the PLC effect, such as activation energy,[10] activation enthalpy,[11] stacking fault energy (SFE),[12] have been studied. Consequently, we wonder whether or not the precipitates could also act as the obstacle to the mobile dislocations and make the PLC effect more pronounced.

Previous study shows that the critical plastic strain of Al alloy is larger as compared with solution-annealed Al alloy,[13] and the PLC effect even completely disappears in some other alloys after long-term aging,[14] whereas the stress drop increases with increasing the aging time.

Until now, an accepted interpretation about this phenomenon has not been achieved. Some researchers hold that the aging process facilitates the precipitation and therefore leads to the lower solute atom concentration in the matrix, which increases the critical plastic strain and retards the PLC effect,[13,14] whereas other researchers hold that the weakened PLC effect stems from the fact that the moving of the mobile dislocations is prevented by the precipitates.[15,16] The latter researchers add that the PLC effect is caused by the process of dislocations cutting the precipitates.[15,16] However, Chemlík *et al.*[17] found that the PLC effect cannot occur if the deformation process is only controlled by dislocation cutting precipitates, and the interaction between solute atoms and dislocations is a necessary condition for the PLC effect. Based on the analyses abovementioned, the relationships between precipitates and the PLC effect need to be further clarified.

As a main strengthening phase in Ni-base superalloys, the γ' precipitates possess some special characteristics, such as dissolve into the γ matrix at high temperature, and reprecipitate and embed in the γ matrix uniformly and coherently at relatively low temperature. Most importantly, structure and composition of the γ' precipitates are not changed in the temperature range of PLC effect normally occurring. On the other hand, the γ' precipitates are of vital important role in plastic deformation. For example, when the γ' precipitates is less than a specific critical size, the deformation mechanism is normally dominated by the dislocation cutting the γ' precipitate, whereas the deformation process transforms to Orowan by-passing mechanism when the size of γ' precipitate is larger than a critical value.[18–22] In the present work, Nimonic 263 Ni-base superalloy is selected and the γ' precipitate with various sizes and volume fractions will be fabricated first through altering the aging treatment.[17] Then the research focus will be given the correlation between the PLC effect and the deformation mechanism influenced by the γ' precipitate, and therefore the role of the γ' precipitate in PLC effect is predicted to be clarified.

II. EXPERIMENTAL PROCEDURE

The nominal chemical composition (wt pct) of Nimonic 263 alloy used in this investigation is listed in Table I. Ingots were prepared by vacuum induction melting (VIM). After 1473 K (1200 °C)/10 h homogenization, the ingots were hot forged at 1373 K (1100 °C) to 30 mm (diam.) bar, and then cut to small bars of 7 mm in diameter and 55 mm in length. The small bars were solution-annealed at 1423 K (1150 °C) for 1.5 hours, and then quenched to room temperature to suppress the precipitation of the γ' phase. Finally, the small bars were aged at 1073 K (800 °C) for different times (0.15, 0.5, 2, 10, 25, 50, 100, 300, and 500 hours). Tensile test specimens with a gage section of 20 mm in length and 3 mm in diameter were machined from the aged alloys. The tensile tests were conducted under a constant strain rate of $4 \times 10^{-4}\ s^{-1}$ at 773 K (500 °C) in air using the INSTRON 5582 mechanical testing machine. Here, at least two tensile specimens under per aging condition were tested, and the tensile behavior of Nimonic 263 alloy under every specific aging condition was well repeated.

In order to measure the variation of the mean radius $\bar{r}(t)$, mean edge-to-edge interprecipitate distance $\bar{L}$, areal number density N_s, and volume fraction V_f of the γ' precipitates with the aging time, the thin foils for transmission electron microscopy (TEM) were prepared by mechanical polishing and twin-jet polishing in a mixture of 10 pct perchloric acid and 90 pct alcohol (v/v). The microstructural configurations of the aged Nimonic 263 alloy were examined using JEM 2100 TEM operated at 200 kV. Under every aging condition, at least three areas were collected. The measurement and statistics of the $\bar{r}(t)$, $\bar{L}$, N_s, and V_f of the γ' precipitates were conducted using the Gatan DigitalMicrograph software. Herein, the effect of the thin film thickness on the volume fraction was neglected, and thus the volume fraction was approximately equal to the area percentage. After the tensile tests, the thin foils for TEM observation were cut 5 mm apart from the fracture surface and polished using the methods as abovementioned. The deformation microstructures were examined using a Tecnai T20 TEM operated at 200 kV.

III. RESULTS

A. *Microstructural Evolution Under Different Aging Times*

Figure 1 shows the microstructures of Nimonic 263 alloy aged at 1073 K (800 °C) for different times. Clearly, no γ' precipitates are observed in the γ matrix even at high magnifications after aging at 1073 K (800 °C) for short time, *e.g.*, 0.15 hour, as shown in Figure 1(a). Prolonging the aging time, spherical γ' precipitates with a diameter of 12 nm are observed (2 hours), as shown in Figure 1(b). With further increasing the aging time, the size and quantity of the γ' phase are changed, whereas the γ' precipitates remain in a spherical shape, as shown in Figures 1(c) and (d). The measurement and statistics of the $\bar{r}(t)$, $\bar{L}$, and N_s of the γ' precipitates as a function of the aging time (over 2 hours) are plotted in Figure 2. Notably, the γ' precipitates cannot be identified when the aging time is less than 2 hours. Clearly, the mean radius $\bar{r}(t)$ of the γ' precipitates linearly increases with increasing the aging time, and corresponds to the basic $\bar{r} \propto t^{1/3}$ kinetics of the Lifshitz–Slyozov–Wagner (LSW) theory.[23,24]

Table I. Nominal Chemical Composition (Wt Pct) of Nimonic 263 Alloy

Alloy	Co	Cr	Mo	Ti	Al	Fe	C	Mn	Si	Ni
Nimonic 263	20	20	5.8	2.1	0.45	0.7	0.06	0.5	0.4	bal

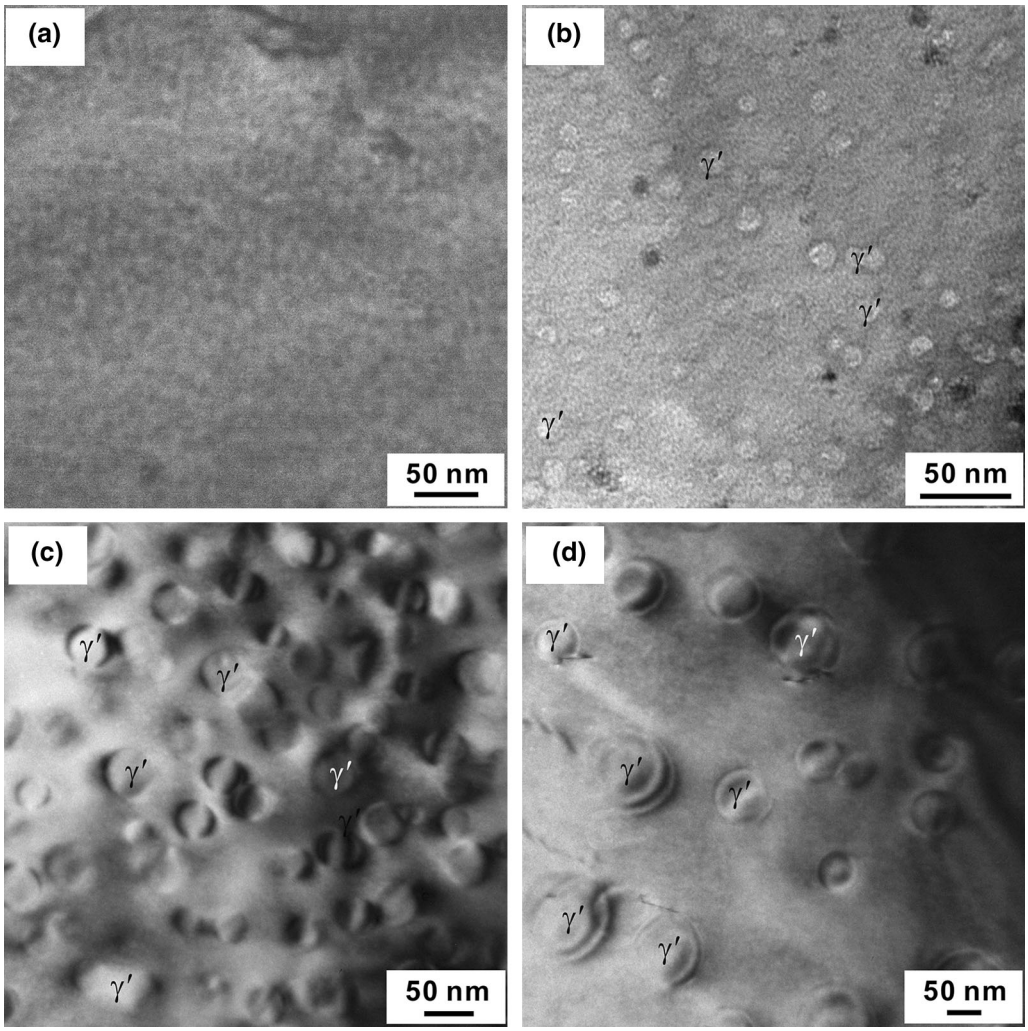

Fig. 1—TEM micrographs of Nimonic 263 alloy aged at 1073 K (800 °C) for 0.15 h (*a*), 2 h (*b*); 50 h (*c*), and 500 h (*d*).

Moreover, the areal number density N_s significantly decreases with increasing the aging time, whereas the mean edge-to-edge interprecipitate distance $\bar{L}$ remarkably increases with increasing the aging time. The variation trends as abovementioned indicate that the microstructural evolution is mainly dominated by the γ' precipitate growing and coarsening after aging 2 hours. Furthermore, the volume fraction of the γ' precipitates rapidly increases to ~14 pct and obtains a maximum volume fraction of ~17 pct (in the thermodynamic equilibrium condition) after aging for 2 and 50 hours, respectively. Further prolonging the aging time, the solute atoms diffuse from the small γ' precipitates to large γ' precipitates leading to the disappearance of the former and the coarsening of the latter, and the volume fraction of the γ' precipitates basically remains constant.

B. *Tensile Behavior-PLC Effect*

Figure 3 shows the true tensile stress–strain curves of the Nimonic 263 alloy with different aging times tested at 773 K (500 °C) with a constant rate of 4×10^{-4} s^{-1}. In order to clearly show the details of the tensile curves, they are elaborately upward or downward translated. Under the current tensile conditions, the PLC effect occurs both in solution-annealed and aging alloys (Figure 3(a)). The serration type changes rapidly from Type B (in solid solution) to Type C with increasing the aging time, as shown in Figure 3(b). The following characteristics are observed from the partial enlarged view of all tensile curves (Figure 3(b)): (i) the stress drop frequency gradually decreases with increasing the aging time, and then increases again when the aging time is over 50 hours; (ii) the critical plastic strain for onset of serrations in solid solution is larger than that under

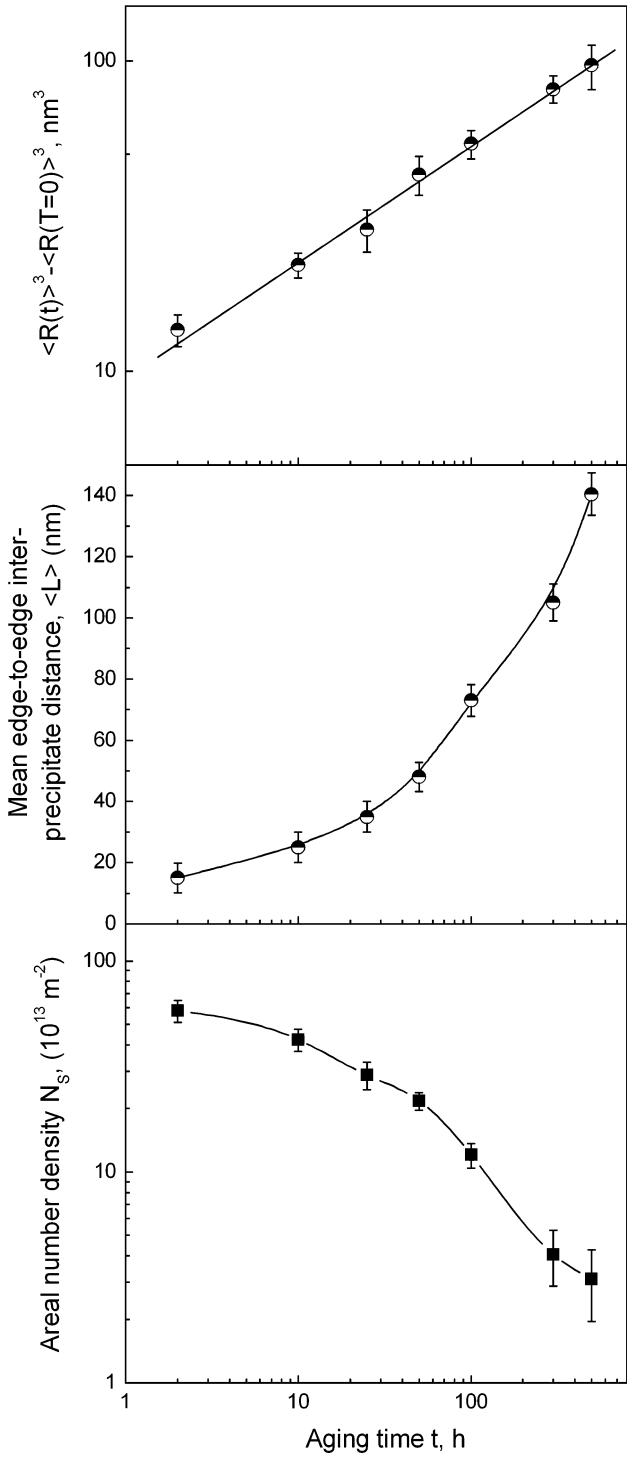

Fig. 2—Variation of the mean radius $\bar{r}(t)$, mean edge-to-edge inter-precipitate distance $\bar{L}$, and areal number density N_s of the γ' precipitates with the aging time.

aging conditions; (iii) the critical plastic strain increases with increasing the aging time and then gradually decreases after reaching the maximum which is obtained after aging for 50 hours, as shown in Figure 4. Notably, the elastic deformation part is removed from the critical strain (in Figure 4).

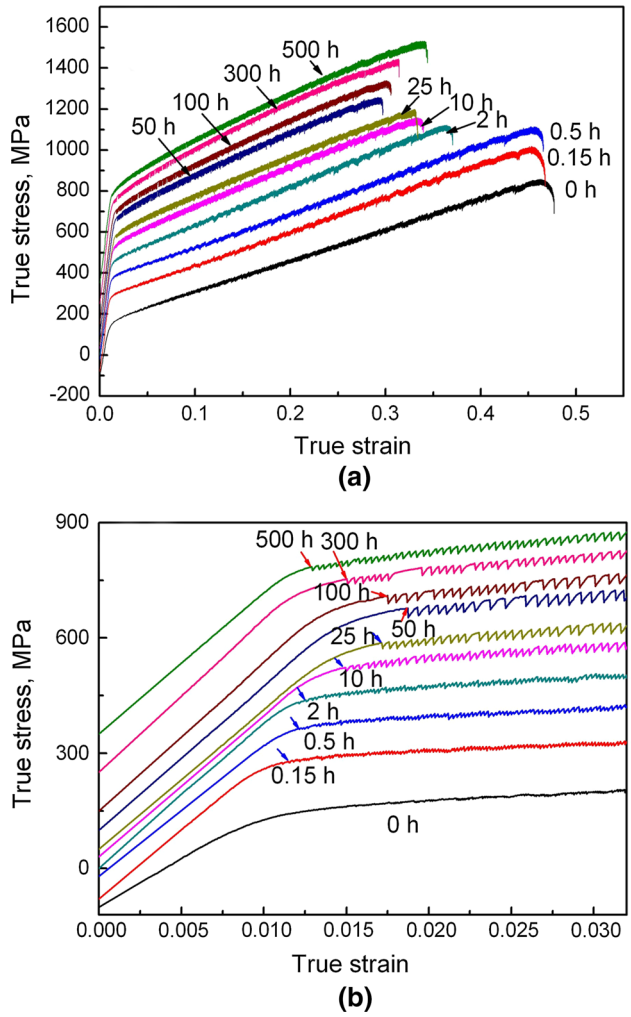

Fig. 3—True stress–strain curves (*a*) and partial magnification of the onset of PLC effect in (*b*) of Nimonic 263 alloy with different aging times after tensile tests at 773 K (500 °C) with a constant strain rate of 4×10^{-4} s^{-1}.

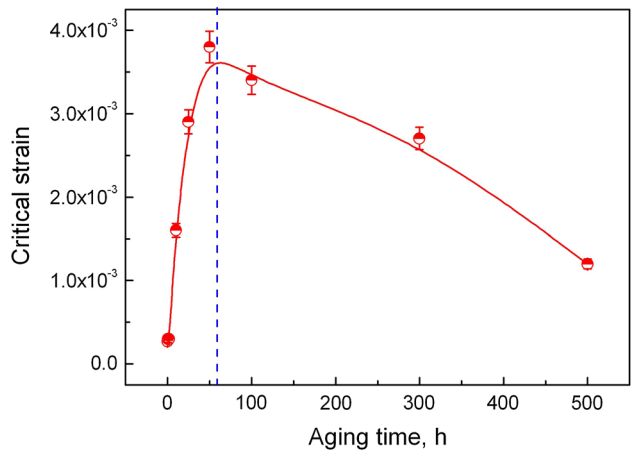

Fig. 4—Variation of critical plastic strain for the onset of the PLC effect with the aging time.

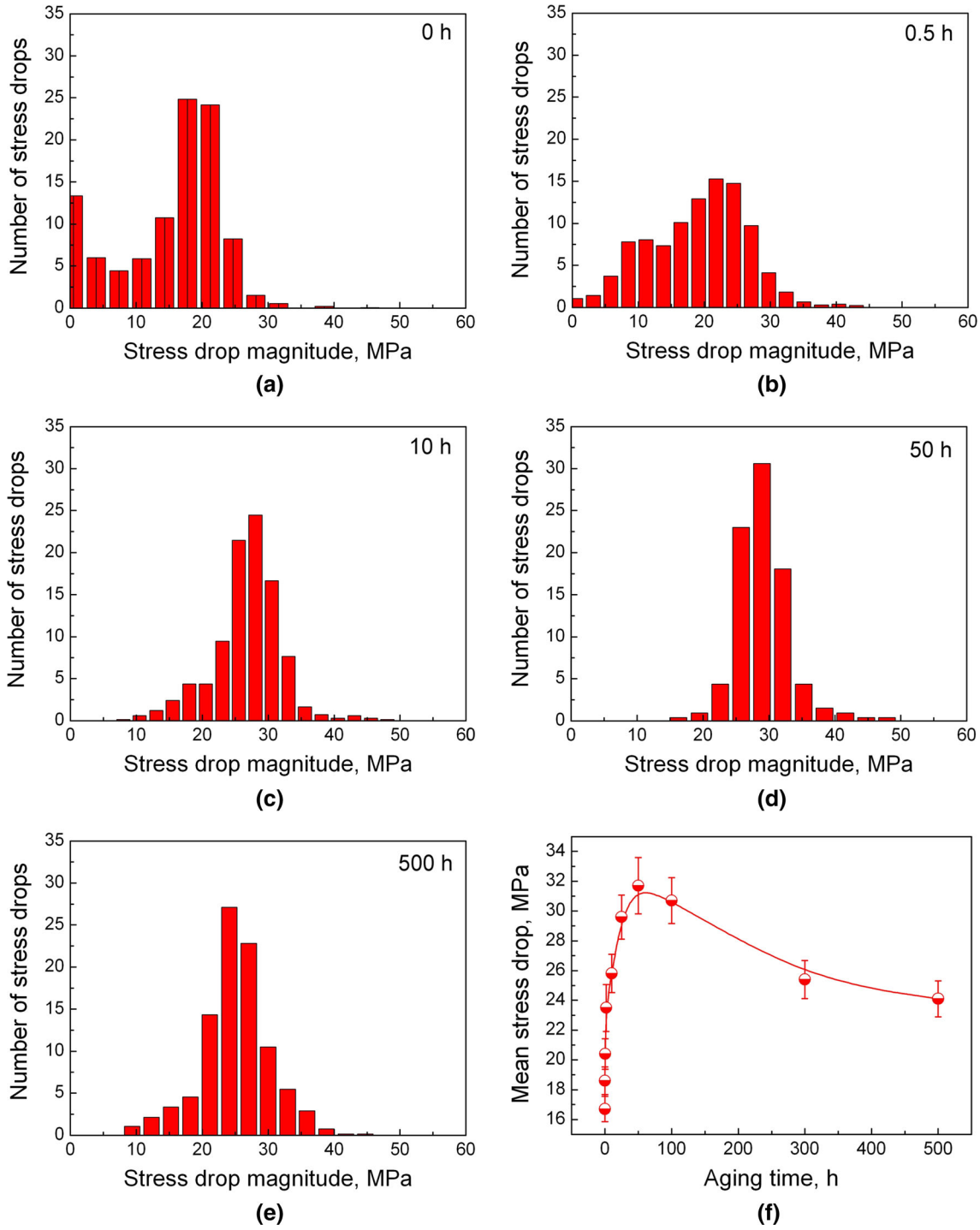

Fig. 5—Statistical histogram of stress drop after different aging times (*a*–*e*) and variation of the mean stress drop with the aging time (*f*).

The statistical distributions of the stress drop magnitude as a function of the aging time are shown in Figure 5. The stress drop in solution-annealed Nimonic 263 alloy (Figure 5(a), 0 hour) shows a transitory stage from the power-law function to the single peak statistical function, and this distribution is corresponding to the serrations of Type B. After aging heat treatment, the stress drop distribution changes to the single peak statistical function with a variation in one side of the peak, *i.e.*, the number of the stress drop on the left of the peak gradually decreases. A symmetrical distribution is observed after aging for 10 hours, as shown in Figure 5(c). Within aging for 0 to 50 hours (Figure 5(a) through (c)), the peak of statistical stress drop distribution gradually moves to the high stress drop side with increasing the aging time (the stress increasing from ~20 to ~30 MPa), whereas it moves to the low stress drop side again with further increasing the aging time (over 50 hours). This situation is clearly reflected by the variation of mean stress drop ($\Delta\sigma$) with

the aging time, as shown in Figure 5(f). The variation trend of mean stress drop with aging time is similar to the critical plastic strain shown in Figure 4. The mean stress drop remarkably increases with increasing the aging time and then gradually decreases after reaching a maximum which is obtained after aging for 50 hours (Figure 5(f)).

Notably, two important parameters which cannot be neglected are the waiting time (t_w) of mobile dislocations at the obstacles which could be interpreted as the time period from being obstructed to breaking away from the obstacles, and the free-flying time (t_f) of mobile dislocations after overcoming the obstacles. Here, the t_w corresponds to the time period from the valley to the next peak on the stress–time (strain) curves, and the t_f corresponds to the time period from the peak to the next valley, as shown in Figure 6(a). The strain change leads to the variation of the density of mobile dislocations and forest dislocations, and therefore the change of t_w and t_f. The variations of the mean waiting time (Δt_w) and mean free-flying time (Δt_f) in the entire strain range are calculated, as shown in Figure 6(b). The variation of the mean waiting time with the aging time is similar with that of the critical plastic strain (Figure 4) and the mean stress drop (Figure 5(f)), and all of them reach the maximum after aging for 50 hour. Clearly, the variation of mean waiting time with the aging time is consistent with the density of the stress drop, and low frequency of the stress drop indicates the mobile dislocations need longer waiting time before the obstacles. However, the variation of mean free-flying time is not significant and fluctuates up and down at ~0.2 seconds.

C. *Deformation Mechanisms*

Figure 7 shows the microstructural configurations of the tensile-tested Nimonic 263 alloy both in solution-annealed condition and in aged condition. Clearly, no γ' precipitates are observed in Nimonic 263 alloy when the aging time is less than 0.5 hour which is consistent with the observation in Figure 1. Typical microstructural configurations of the low SFE are observed in Figure 7. The low SFE makes it difficult for dislocations to slip in planes different from the plane containing their Burgers vector. Nevertheless, a three-dimensional distribution of dislocations is still observed in Figure 7(a). The a/2⟨101⟩ matrix dislocations of different slip systems are activated during the tensile deformation. These dislocations react and tangle with each other during slipping in the γ solid solution. Actually, the deformation microstructure of the Nimonic 263 alloy under solid solution state is relatively homogeneous and no significant deformation localization is observed. However, with increasing the aging time, a number of dislocation arrays with different pile-up directions are observed (Figure 7(b)), indicating the distribution of dislocations is strictly two-dimensional or planar. Notably, the deformation localization becomes significant and the SBs are gradually evolved, as shown in Figure 7(b). After aging for 10 h, a large amount of small γ' precipitates are observed (Figure 7(c)). However, the tensile deformation mechanisms are still dominated by the formation of SBs,

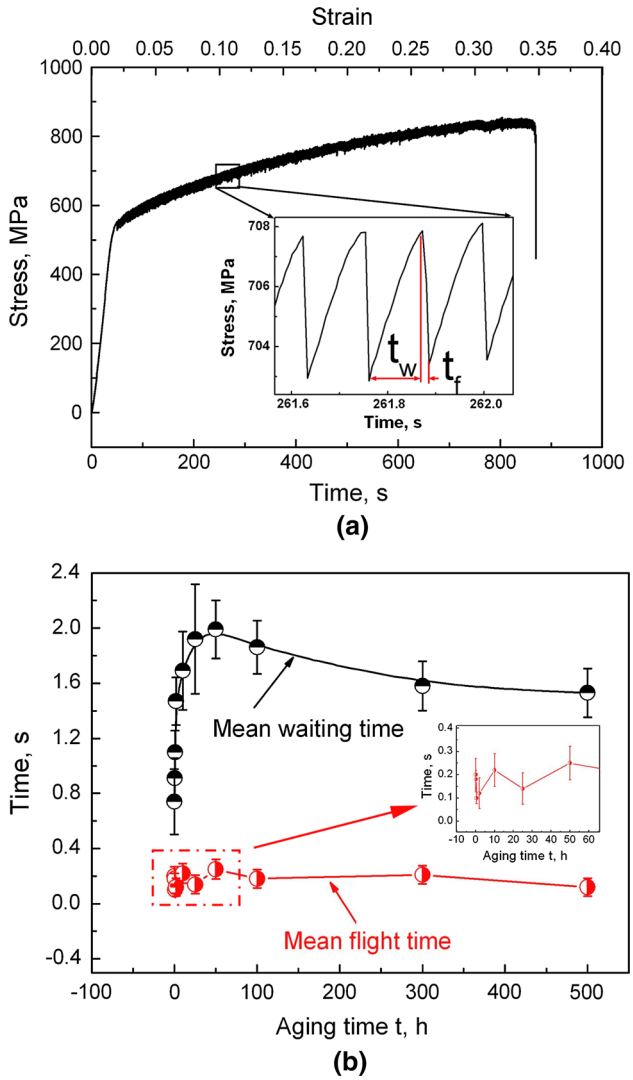

Fig. 6—Illustration of the waiting time (t_w) and the free-flying time (t_f) in the tensile stress–time (strain) curve of Nimonic 263 alloy (*a*); Variation of the mean waiting time and the mean free-flying time of mobile dislocations spends at the obstacles before and after breaking away from them with the aging time (*b*).

revealing the small γ' precipitates are sheared by the APB-coupled pairs of a/2⟨101⟩ type dislocations (APB: Anti-phase domain boundary).

Further increasing the aging time, the a/6⟨112⟩ Shockley partial dislocation continuously shearing the γ and γ' phases (leaving continuous stacking faults (SFs) in γ and γ' phases[25]) in some areas are observed (not shown here), indicating aging for 25 hours is a deformation mechanism transition time range from APB-coupled dislocations shearing to Shockley partial dislocation shearing. Undoubtedly, the a/6⟨112⟩ Shockley partial dislocation shearing becomes an important deformation mechanism after aging for 50 hours (Figure 7(d)). Interestingly, Orowan by-passing mechanism occurs after aging for 50 hours, and the leaving dislocation loops around the γ' precipitates are observed, as marked by arrows in Figure 7(d). In order to clearly show dislocation by-passing process, a TEM specimen near the threaded portion (with a small

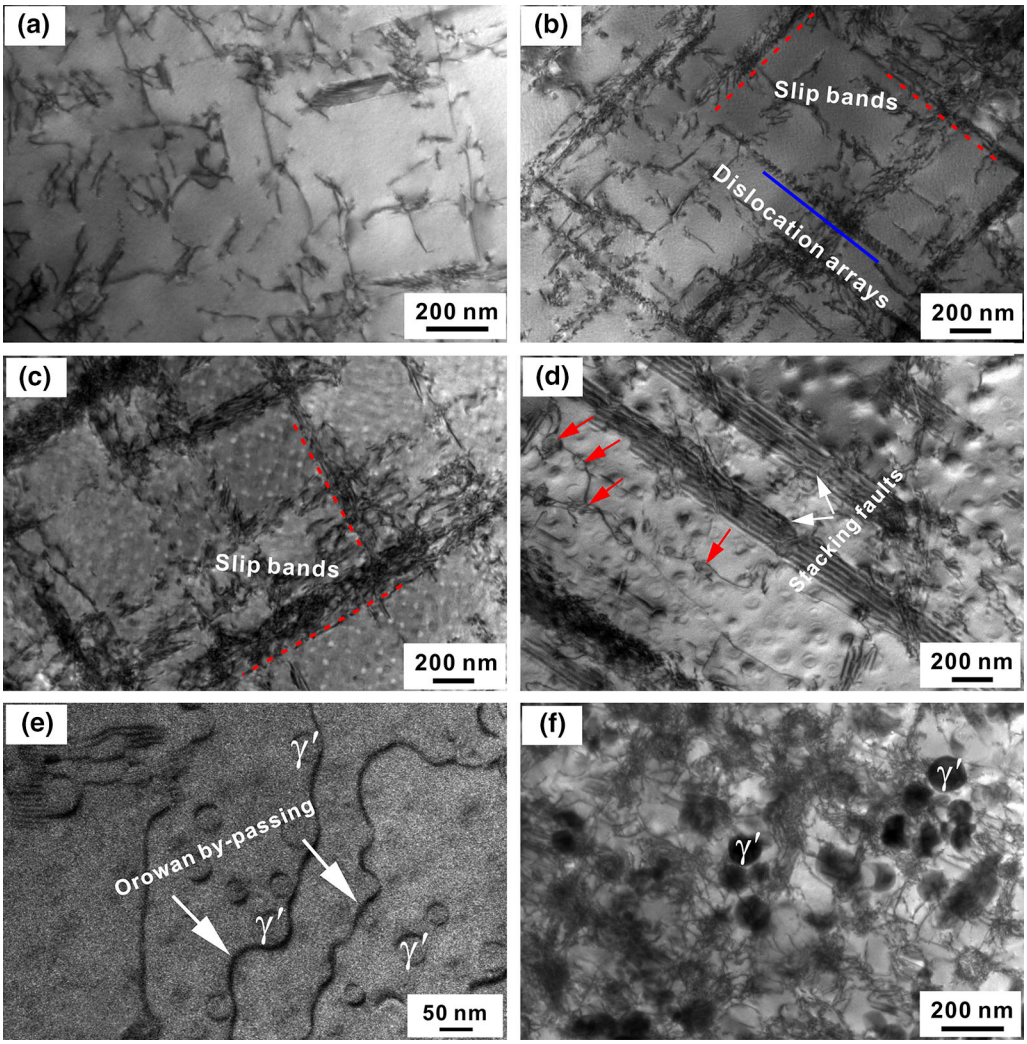

Fig. 7—Microstructural configurations of the Nimonic 263 alloy after tensile tests at 773 K (500 °C) and 4 × 10^{-4} s^{-1} after aging for 0 h (*a*), 0.5 h (*b*), 10 h (*c*), 50 h (*d*, *e*), and 500 h (*f*).

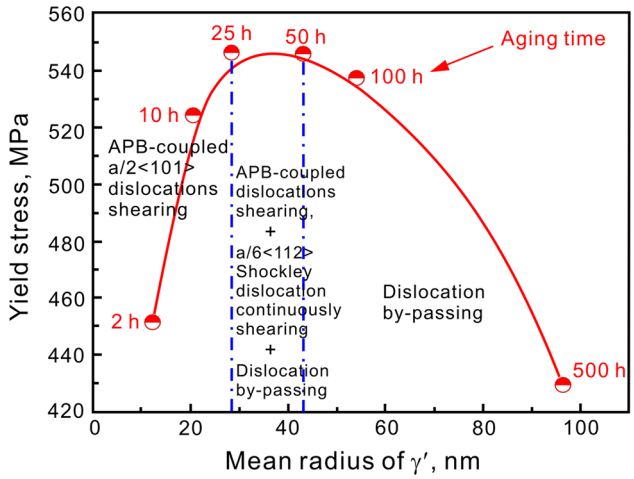

Fig. 8—The effect of the γ' precipitate mean radius on the deformation mechanism and the yield stress.

deformation) was examined. Orowan by-passing process is frequently observed in some regions where the edge-to-edge interprecipitate distance is large, indicating the deformation mechanisms change from the APB-coupled a/2⟨101⟩ dislocations shearing to the a/6⟨112⟩ Shockley partial dislocation shearing and a/2⟨101⟩ matrix dislocation by-passing the γ' precipitates, as shown in Figure 7(e). However, the APB-coupled pairs of a/2⟨101⟩ type dislocations shearing still cannot be neglected. Therefore, the deformation mechanism after aging for 50 hours is a mixed mechanism. After aging for 500 hours, the deformation mechanisms are dominated by the dislocation by-passing mechanism (the γ' precipitates are surrounded by dislocation loops), and the deformation becomes more homogenous, as shown in Figure 7(f).

The dependence of the deformation mechanisms on the mean radius of γ' and the yield stress is summarized in Figure 8. Notably, the γ' precipitates' size change caused by different aging times leads to obvious difference of the yield stress. Therefore, in the work reported in this manuscript the relationship between the mean γ' radius and the main deformation mechanisms is considered. As abovementioned, the deformation mechanisms gradually change after aging for 25 and 50 hours, respectively, and

this change is attributed to the variation of the γ' size. In the aged Nimonic 263 alloy with the γ' precipitate mean radius of less than 28 nm (corresponding to the aging time less than 25 hours), the deformation mechanisms are dominated by dislocations slipping in the γ matrix, APB-coupled a/2⟨101⟩ dislocations shearing the small γ' precipitates and the SBs continuously cutting the γ and γ' phases. When the γ' size is between 28 to 45 nm (corresponding to the aging time between 25~50 hours), the deformation mechanism is controlled by the APB-coupled pairs of a/2⟨101⟩ type dislocations shearing γ' precipitates, the Shockley partial dislocation continuously shearing the γ and γ' phases together with matrix dislocations by-passing the γ' precipitates. When the γ' size is over 45 nm (corresponding to the aging time more than 50 hours), the deformation mechanism is mainly controlled by Orowan by-passing process. Obviously, the changes of deformation mechanism must be correlated with the PLC effect. The detailed analyses will be conducted in the following sections.

IV. DISCUSSION

A. *The Dependence of PLC Effect on the γ' Precipitates*

According to the variation of PLC characteristic parameters including the critical plastic strain (Figure 4), the mean stress drop (Figure 5(f)), and the mean waiting time (Figure 6(b)) as a function of the aging time, the microstructural evolution and deformation mechanism changing show significant impact on the PLC effect. After a comprehensive comparison of the tensile curves (Figure 3) and corresponding deformation microstructures (Figure 7), we could find that the PLC effect occurs in Nimonic 263 alloy regardless of whether the deformation mechanism is manipulated by dislocation of the shearing or the by-passing of the γ' precipitates. Therefore, a conclusion can be drawn that the dislocation shearing mechanism is not the requirement for the PLC effect occurring.

As analyzed in "Section III–C", when the deformation mechanism transforms from APB-coupled a/2⟨101⟩ dislocation shearing to the mixed form (Shockley partial dislocation continuously cutting the γ and γ' phases combined with matrix dislocations by-passing the γ' precipitates), the yield strength remarkably increases (Figure 8). However, the yield strength drops dramatically when the deformation mechanism transforms to Orowan by-passing from the mixed deformation mechanism. These variations indicate that the hindering effects of the obstacles for mobile dislocations strengthen initially and then weaken gradually during the deformation mechanism transformation. Clearly, two aspects are directly reflected by these hindering effects, *i.e.*, (i) the mean waiting time of mobile dislocations at the obstacles and (ii) the mean stress drop. The variations of the mean waiting time and mean stress drop are consistent with the change of the hindering effects of γ' precipitates to the mobile dislocations. It is considered that the mobile dislocations move in an intermittent mode, *i.e.*, dislocations may be obstructed by obstacles and they will move rapidly between adjacent obstacles. When the movement of the mobile dislocations is impeded by the γ' precipitates, the loading stress must be high enough for the mobile dislocations to overcome this obstacle by shearing or by-passing mechanism. Here, the time of mobile dislocations impeded by the γ' precipitates is considered to be the waiting time (t_w) of mobile dislocations at the obstacles. Notably, the waiting time (t_w) of mobile dislocations is closely related to the volume fraction, size, and edge-to-edge interprecipitate distance of the γ' precipitates. Therefore, when the hindering effects caused by the γ' precipitates are the most significant, the corresponding waiting time (t_w) reaches the maximum (the mean size of γ' precipitates is about 45 nm). The solutes rapidly gather at the arrested dislocations by preferred pipe diffusion (some researchers believe that this occurs *via* other types of diffusion[26,27]) simultaneously. Because of the longest waiting time, the concentration of the solutes clustered at the mobile dislocations is very high, and the mobile dislocations are effectively pinned. With the aid of applied stress, the pinned dislocations escape from the solute by a thermal activation process. The collective and synchronous unpinning in a local area brings about a maximum mean stress drop after aging 50 hours. Therefore, a conclusion is drawn from the variation of the mean waiting time and the mean stress drop that the γ' precipitates only retard the movement of the mobile dislocations. After overcoming the γ' precipitates by shearing or by-passing and escaping from the solute atmospheres by the thermal activation process, these pinned mobile dislocations continually move forward.

B. *The Relationships Between Critical Plastic Strain and Deformation Mechanisms*

For the second phase strengthened alloys, it is generally considered that the formation mechanisms of the PLC effect agree well with the M–K model,[5] *i.e.*, the PLC effect results from the interactions between the mobile dislocations and the solute atoms gathering at the forest dislocations. The density of mobile dislocations is reduced, and the waiting time at the forest dislocations is increased due to the hindering effect of the γ' precipitates. The factors which cause the decrease of the mobile dislocation density are as follows: (i) the hindering effects of the second phase and grain boundary to the mobile dislocations, (ii) the mutual annihilation of the mobile dislocations with opposite Burgers vector, and (iii) the mobile dislocations move to the crystal surface. Clearly, for the γ' phase strengthened Nimonic 263 alloy, the hindering effects of the γ' precipitates are responsible for the decreasing of the mobile dislocation density. Herein, aging for 50 hours (the mean size of the γ' precipitates is about 45 nm) is considered as a critical state. Aging less than 50 hours, with the volume fraction and size of the γ' precipitates increasing, the deformation mechanisms gradually change from APB-coupled a/2⟨101⟩ dislocations shearing to Shockley partial dislocation continuously shearing, and the hindering effects of the γ' precipitates are gradually strengthened. Therefore, the density of the mobile dislocations which can overcome the solute atom

pinning effects decreases with increasing the aging time. Although the volume fraction of the γ' precipitates remains the same after aging for more than 50 hours, the number density and the size of the γ' precipitates decreases and increases (Figure 2), respectively. Consequently, the density of mobile dislocations which can overcome the solute atom pinning slightly increases again. Notably, it is difficult to quantitatively express the change of the mobile dislocation density using a mathematical model because of the difference in deformation mechanisms. However, the correlations between the microdeformation mechanisms and macro-PLC effect are well explained by the Kubin–Estrin model.[28] Herein, the Kubin–Estrin model is also used to explain the dependence of the critical strain on the aging time. It is considered that the negative strain rate sensitivity (nSRS) is the requirement for the PLC effect occurring.[28–30] The total strain rate sensitivity, S, is given by [28]

$$S = S_0 + S_{\text{aging}} = S_0 - \frac{2}{3}\sigma_0(t_w/\tau_0)^{2/3}\exp[-(t_w/\tau_0)^{2/3}]. \quad [1]$$

Here, S_0 generally is a variable quantity and proportional to stress and strain, however, for the sake of simplicity, S_0 will be considered constant. S_{aging} is the contribution of DSA to the total S. σ_0 is the maximum increase in stress which is produced by the aging mechanism and τ_0 is the relaxation time associated with diffusion which depends on the binding energy between a solute atom and a dislocation, on the diffusion coefficient of solute atoms and on solute concentration.

The critical condition for the PLC effect occurring is $S < 0$, and we can obtain

$$X\exp(-X) > \alpha \quad [2]$$

where $\alpha = \frac{3}{2}(S_0/\sigma_0)$ and $X = (t_w/\tau_0)^{2/3} = (\Omega/Z)^{2/3}$, with $Z = \dot{\varepsilon}\tau_0$ and thus, $\Omega = \dot{\varepsilon}t_w$. Here, Ω is the elementary incremental strain and $\dot{\varepsilon}$ is the strain rate. Depending on the value of α, Eq. [2] defines two solutions, X_1 and X_2 ($X_2 > X > X_1$). Therefore, the requirement for nSRS is given as[28]

$$\tau_0 X_1^{3/2} < t_w < \tau_0 X_2^{3/2}, \quad [3]$$

where the waiting time is given by

$$t_w = \frac{\rho_f^{-1/2}\rho_m b}{\dot{\varepsilon}} \quad [4]$$

Here, b is the Burgers vector, and ρ_m and ρ_f are the densities of mobile and forest dislocations, respectively. Consequently, a variation of the elementary incremental strain (Ω) with the strain at different aging times is expressed as follows:

$$\Omega = \dot{\varepsilon}t_w = b\rho_m\rho_f^{-1/2}. \quad [5]$$

According to Eq. [5], Eq. [3] is transformed to

$$\tau_0\dot{\varepsilon}X_1^{3/2} < \Omega < \tau_0\dot{\varepsilon}X_2^{3/2} \quad [6]$$

As a consequence, two critical values, $\Omega_1 = \tau_0\dot{\varepsilon}X_1^{3/2}$ and a, for the PLC effect that occurs are obtained. In other words, only when Ω lies in the interval of $[\Omega_1, \Omega_2]$, the PLC effect occurs, as shown in Figure 9.

With increasing the aging time, the density of mobile dislocations decreases, and the curve of the elementary incremental strain (Ω) versus the strain (ε) moves towards to the bottom right. Therefore, the requirement $\Omega = \Omega_1$ should to be satisfied if the PLC effect occurs. Clearly, the critical strain increases ($\varepsilon_4 > \varepsilon_3 > \varepsilon_2 > \varepsilon_1$) with increasing the aging time (within 50 hours). Here, the strains ε_1, ε_2, ε_3, and ε_4 shown in Figure 9 are corresponding to the critical strain after aging for 2, 10, 25, and 50 hours, respectively (these critical strains consistent with that in Figure 4). When the aging time is over 50 hours, the main deformation mechanisms gradually change from dislocation shearing to dislocation by-passing the γ' precipitates. The density of the mobile dislocations is related to the interprecipitate distance. When the interprecipitate distance increases with increasing the aging time, the mobile dislocations can by-pass the γ' precipitates more easily and its density increases again. Thus, the curves of Ω versus ε move towards to the top left, and thus the critical plastic strain for the onset of the PLC effect gradually decreases again ($\varepsilon_5 < \varepsilon_2 < \varepsilon_3 < \varepsilon_4$).

Clearly, the relationships between the critical plastic strain and deformation mechanisms are well established by Eq. [1]. In fact, the viewpoint of effects of precipitates on the density of mobile dislocations leading to inverse PLC effect has been proposed in the previous work.[31] However, no good evidence has been provided in the past decades. Herein, although the deformation mechanisms of inverse PLC effect at high temperatures or low strain rates are not examined, the critical plastic strain as a function of the aging time can indirectly prove that the inverse PLC effect relates to the decreasing of the mobile dislocation density.

The results of present investigation show that dislocation shearing and by-passing deformation mechanisms are important but not the essential reasons of the PLC effect. The interactions among solutes atoms, mobile dislocations, and forest dislocations are the

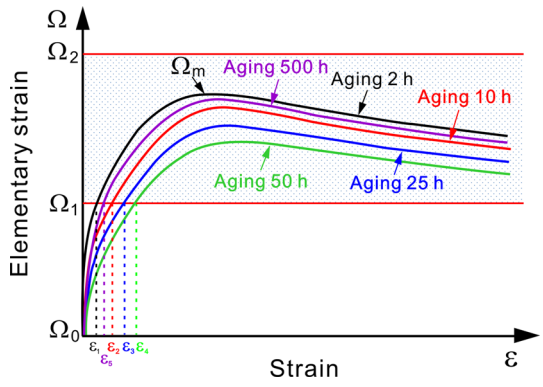

Fig. 9—Schematic illustration of the strain dependence of the critical strains with increasing the aging time for Nimonic 263 alloy. Strains ε_1, ε_2, ε_3, ε_4, and ε_5 are corresponding to the critical strain after aging for 2, 10, 25, 50, and 500 h, respectively (these critical strains consistent with that in Fig 4).

essential reasons for the onset of PLC effect. However, the precipitation process of the γ' phase can directly influence the PLC effect by changing the abovementioned interactions.

V. CONCLUSIONS

In this work, the dependence of PLC effect on the γ' precipitates of the Nimonic 263 alloy with different aging times has been studied by analyzing the parameters of the tensile curves and the deformation mechanisms. The following conclusions can be drawn from this work:

(1) The γ' precipitates with different sizes, edge-to-edge interprecipitate distance, and areal number density are obtained by altering the aging time. The γ' precipitates cannot be observed when the Nimonic 263 alloy is aged less than 2 hours.

(2) When the mean size of the γ' precipitates is less than 28 nm (aging less than 25 hours), the deformation mechanisms are dominated by APB-coupled $a/2\langle 101\rangle$ dislocations shearing the small γ' precipitates and the SBs continuously cutting the γ and γ' phases. When the γ' size is between 28 and 45 nm (aging time between 25 and 50 hours), the deformation mechanism is controlled by the APB-coupled pairs of $a/2\langle 101\rangle$ type dislocations shearing γ' precipitates, the $a/6\langle 112\rangle$ Shockley partial dislocation continuously shearing the γ and γ' phases combined with matrix dislocations by-passing the γ' precipitates. When the γ' size is over 45 nm (aging time more than 50 hours), Orowan by-passing becomes the main deformation mechanism.

(3) The critical plastic strain for the onset of the PLC effect shows an increasing tendency with increasing the aging time, and then gradually decreases after reaching the maximum. The dependence of the mean stress drop and waiting time on the aging time shows an extremely similar tendency with that of the critical plastic strain.

(4) The dependence of the critical plastic strain on the deformation mechanisms is well explained by the elementary incremental strain (Ω). The dislocation shearing and by-passing deformation mechanisms are important but not the essential reasons of the PLC effect. The precipitation process of the γ' phase can directly influence the PLC effect by changing the interactions among solutes atoms, mobile dislocations, and forest dislocations.

ACKNOWLEDGMENTS

The financial support provided by the High Technology Research and Development Program of China (No. 2014AA041701) and the National Natural Science Foundation of China (NSFC) under Grant Nos. 51171179, 11332010, 51271174, and 51401210 for carrying out the present research work is gratefully acknowledged. The authors are grateful to Zhiwu Shi (Institute of Metal Research) for the useful discussions.

REFERENCES

1. A.H. Cottrell: *Philos. Mag*., 1953, vol. 44, pp. 829–32.
2. P.G. McCormick: *Acta Metall*., 1972, vol. 20, pp. 351–54.
3. A.V.D. Beukel: *Phys. Status Solid*, 1975, vol. 30, pp. 197–206.
4. C. Cornet, K. Wackermann, C. Stöcker, H.-J. Christ, C. Lupton, M. Hardy, and J. Tong: *Met High Temp*, 2014, vol. 31, pp. 226–32.
5. R.A. Mulford and U.F. Kocks: *Acta Metall*., 1979, vol. 27, pp. 1125–34.
6. K. Gopinath, A.K. Gogia, S.V. Kamat, and U. Ramamurty: *Acta Mater*., 2009, vol. 57, pp. 1243–53.
7. S.H. Fu, T. Cheng, Q.C. Zhang, Q. Hu, and P.T. Cao: *Acta Mater*., 2012, vol. 60, pp. 6650–65.
8. G.M. Han, C.G. Tian, Z.K. Chu, C.Y. Cui, Z.Q. Hu, and X.F. Sun: *Metall. Mater. Trans. A*, 2015, vol. 46A, pp. 4629–35.
9. B. Max, B. Viguier, E. Andrieu, and J.M. Cloue: *Metall. Mater. Trans. A*, 2014, vol. 45A, pp. 5431–41.
10. P. Fernandez-Zelaia, B.S. Adair, V.M. Barker, and S.D. Antolovich: *Metall. Mater. Trans. A*, 2015, vol. 46A, pp. 5596–5609.
11. T.E. Moss and G.S. Was: *Metall. Mater. Trans. A*, 2012, vol. 43A, pp. 3428–32.
12. C.Y. Cui, C.G. Tian, Y.Z. Zhou, T. Jin, X.F. Sun: in *Superalloys 2012*, E.S. Huron, R.C. Reed, M.C. Hardy, M.J. Mills, R.E. Montero, P.D. Portella, J. Telesman, eds., TMS, Warrendale, PA, 2012, pp. 715–22.
13. D.L. Sun, D.Z. Yang, and T.Q. Lei: *Mater. Chem. Phys*., 1990, vol. 25, pp. 307–13.
14. S.A. Nalawade, M. Sundararaman, R. Kishorea, and J.G. Shah: *Scripta Mater*., 2008, vol. 59, pp. 991–94.
15. S. Kumar and E. Pink: *Scripta Metall. Mater*., 1995, vol. 32, pp. 749–53.
16. S. Kumar and H.B. McShane: *Scripta Metall. Mater*., 1993, vol. 28, pp. 1149–54.
17. F. Chmelík, E. Pink, J. Król, J. Balík, J. Pešička, and P. Lukáč: *Acta Mater*., 1998, vol. 46, pp. 4435–42.
18. C.Y. Cui, Y.F. Gu, Y. Yuan, T. Osada, and H. Harada: *Mater. Sci. Eng. A*, 2011, vol. 528, pp. 5465–69.
19. Y. Yuan, Y.F. Gu, T. Osada, Z.H. Zhong, T. Yokokawa, and H. Harada: *Scripta Mater*., 2012, vol. 67, pp. 137–40.
20. T. Osada, Y.F. Gu, N. Nagashima, Y. Yuan, T. Yokokawa, and H. Harada: *Acta Mater*., 2013, vol. 61, pp. 1820–29.
21. B.D. Fu, K. Du, G.M. Han, C.Y. Cui, and J.X. Zhang: *Mater. Lett*., 2015, vol. 152, pp. 272–75.
22. C.Y. Cui, Y.F. Gu, Y. Yuan, and H. Harada: *Scripta Mater*., 2011, vol. 64, pp. 502–05.
23. I.M. Lifshitz and V.V. Slyozov: *Phys. Chem. Solids*., 1961, vol. 19, pp. 35–50.
24. A.J. Ardell: *Acta Metall*., 1972, vol. 20, pp. 61–71.
25. B. Décamps, S. Raujol, A. Coujou, F. Pettinari-Sturmel, N. Clément, D. Locq, and P. Caron: *Philos. Mag*., 2004, vol. 84, pp. 91–107.
26. R.C. Picu: *Acta Mater*., 2004, vol. 52, pp. 3447–58.
27. W.A. Curtin, D.L. Olmsted, and L.G. Hector, Jr: *Nat. Mater*., 2006, vol. 5, pp. 875–80.
28. L.P. Kubin and Y. Estrin: *Acta Metall. Mater*., 1990, vol. 38, pp. 697–708.
29. P. Penning: *Acta Metall*., 1972, vol. 20, pp. 1169–75.
30. C.P. Ling and P.G. McCormick: *Acta Metall. Mater*., 1993, vol. 41, pp. 3127–31.
31. J. Guillot and J. Grilhe: *Acta Metall*., 1972, vol. 20, pp. 291–95.